



CHORUS

This is the accepted manuscript made available via CHORUS. The article has been published as:

Electroweak production of top-quark pairs in e^+e^- annihilation at NNLO in QCD: The vector current contributions

Jun Gao and Hua Xing Zhu

Phys. Rev. D **90**, 114022 — Published 17 December 2014

DOI: [10.1103/PhysRevD.90.114022](https://doi.org/10.1103/PhysRevD.90.114022)

Electroweak production of top-quark pairs in e^+e^- annihilation at NNLO in QCD: the vector contributions

Jun Gao

Department of Physics, Southern Methodist University, Dallas, TX 75275-0181, USA

Hua Xing Zhu

*SLAC National Accelerator Laboratory,
Stanford University, Stanford, CA 94309, USA*

Abstract

We report on a calculation of the vector current contributions to the electroweak production of top quark pairs in e^+e^- annihilation at next-to-next-to-leading order in Quantum Chromodynamics. Our setup is fully differential and can be used to calculate any infrared-safe observable. The real emission contributions are handled by a next-to-next-to-leading order generalization of the phase-space slicing method. We demonstrate the power of our technique by considering its application to various inclusive and exclusive observables.

1. Introduction

Continuum electroweak production of top quark pairs at future linear colliders is of considerable interest because it allows for a precise measurement of the top quark forward-backward asymmetry. This observable is of particular importance because it is expected to severely constrain anomalous couplings which could potentially appear in the top quark sector [1]. In the near future, due to the extremely clean environment expected at proposed e^+e^- colliders, it should be possible to measure the top quark forward-backward asymmetry to a precision of approximately 1% [2].

At an e^+e^- collider, top quark pairs are primarily produced via the electroweak process

$$e^+e^- \rightarrow \gamma^*/Z^* \rightarrow t\bar{t}. \quad (1)$$

In this paper, we shall only concern ourselves with the next-to-next-to-leading order (NNLO) radiative corrections to the above process in Quantum Chromodynamics (QCD) mediated by an off-shell photon (γ^*). In other words, we treat the vector current contributions to the production of a top-antitop pair. Complete results including the axial-vector contributions (*i.e.* that due to off-shell Z boson exchange) will be presented elsewhere.

The calculation of QCD radiative corrections to heavy-quark pair production in e^+e^- annihilation has a long history. Full next-to-leading order (NLO) QCD corrections were first computed in ref. [3] and, a short time later, NLO electroweak effects were considered in ref. [4]. NLO QCD corrections to top quark pair production including the subsequent top quark decays were presented in ref. [5] and NLO QCD corrections to top quark spin correlations were computed in refs. [6] and [7]. Total cross sections are known to NNLO in the threshold expansions [8–12] and high-energy expansions [13–17]. Results for the forward-backward asymmetry are also known in the small mass approximation [18–20]. In the near future, the threshold cross section at NNNLO will also be available [21–23]. Somewhat surprisingly, although a great deal of theoretical progress has been made over the years, exact NNLO QCD calculations for fully differential $e^+e^- \rightarrow t\bar{t}$ observables remain a challenge and are still missing from the literature.

A fully differential NNLO QCD calculation is naturally split up into three distinct parts, depending on the number of particles that appear in the final state relative to leading order: a) purely virtual two-loop or squared one-loop corrections, b) one-loop, single-emission

real-virtual corrections, and c) double-emission double-real corrections. For $e^+e^- \rightarrow t\bar{t}$, significant progress has been made in recent years towards the calculation of each of these three pieces. NLO QCD corrections to heavy quark pair production in association with one additional jet were computed in refs. [24–28]. The two-loop heavy quark form factor was first obtained in refs. [29–31] and then confirmed some time later by an independent calculation [32]. In fact, for quite some time, the only outstanding problem was to construct an efficient framework for the combination of the ingredients described above into an infrared-safe Monte Carlo event generator.

For generic processes, this is highly non-trivial due to the fact that, in phase space regions where soft and/or collinear limits are approached, the real-virtual and double-real contributions develop soft and/or collinear divergences which must be extracted before a Monte Carlo integration over phase space can be carried out. At NLO, this is relatively straightforward to do and both phase-space slicing [33–39] and subtraction [40–45] techniques which solve the problem were worked out long time ago. However, as is clear from the massive amount of literature on the subject [46, 47, 58–111], analogous techniques at NNLO are considerably more complicated to develop and complete solutions took much longer to emerge. For example, in the important case of massless dijet production, it took more than a decade for the first physical predictions to appear [46, 47] from the time that the relevant two-loop virtual amplitudes were first calculated [48–57]. As a result of significant theoretical efforts during the past decade, a number of important “benchmark processes” are now known to NNLO [46, 47, 96, 103, 104, 110].

The goal of this paper is to study fully differential NNLO QCD corrections to $e^+e^- \rightarrow t\bar{t}$ using a higher-order generalization of the phase-space slicing method. While we constrain ourselves in this paper to present results for the vector current contributions by themselves, the formalism developed here can, if desired, readily be used to calculate the contributions coming from the exchange of an off-shell Z boson. This paper is organized as follows. In Section 2, we describe our calculational method in detail. In Section 3, we present numerical results for various inclusive and differential observables and, whenever possible, compare them to the existing literature. Finally, we conclude in Section 4.

2. Phase-space slicing at NNLO

We explain in detail our generalization of phase-space slicing method in dealing with the specific process $e^+e^- \rightarrow t\bar{t}$ at NNLO. As mentioned before, there are three distinct parts contribute to the cross section at $\mathcal{O}(\alpha_s^2)$,

$$\begin{aligned} \sigma^{(2)} = & \int d\Phi_{t\bar{t},0} \sum_{\text{spin,color}} \left[2\Re \left(\mathcal{M}_{e^+e^- \rightarrow t\bar{t}}^{(0)} \left(\mathcal{M}_{e^+e^- \rightarrow t\bar{t}}^{(2)} \right)^* \right) + \left| \mathcal{M}_{e^+e^- \rightarrow t\bar{t}}^{(1)} \right|^2 \right] \\ & + \int d\Phi_{t\bar{t},1} \sum_{\text{spin,color}} \left[2\Re \left(\mathcal{M}_{e^+e^- \rightarrow t\bar{t}g}^{(0)} \left(\mathcal{M}_{e^+e^- \rightarrow t\bar{t}g}^{(1)} \right)^* \right) \right] \\ & + \int d\Phi_{t\bar{t},2} \sum_{\text{spin,color}} \left[\left| \mathcal{M}_{e^+e^- \rightarrow t\bar{t}gg}^{(0)} \right|^2 + \left| \mathcal{M}_{e^+e^- \rightarrow t\bar{t}q\bar{q}}^{(0)} \right|^2 \right], \end{aligned} \quad (2)$$

where

$$\begin{aligned} d\Phi_{t\bar{t},n} = & \frac{1}{2s \times 2^2} \left(\frac{d^{D-1}p_t}{2E_t(2\pi)^{D-1}} \right) \left(\frac{d^{D-1}p_{\bar{t}}}{2E_{\bar{t}}(2\pi)^{D-1}} \right) \\ & \times \prod_{i=1}^n \left(\frac{d^{D-1}p_i}{2E_i(2\pi)^{D-1}} \right) (2\pi)^D \delta^{(D)} \left(Q - p_t - p_{\bar{t}} - \sum_{i=1}^n p_i \right) \end{aligned} \quad (3)$$

is the phase space volume element in $D = 4 - 2\epsilon$ dimension, divided by the flux factor and initial state spin average factor. Here $s = Q^2 = (p_{e^+} + p_{e^-})^2$ is the center-of-mass energy square. $\mathcal{M}_{e^+e^- \rightarrow t\bar{t}...}^{(i)}$ denotes the i -loop amplitude for $e^+e^- \rightarrow t\bar{t}$ plus zero, one, or two additional massless partons. Note that when $\sqrt{s} > 4m_t$, the channel for the production of $t\bar{t}\bar{t}$ is open. However, these additional contributions are themselves infrared finite due to the mass of top quark, and can be dealt with separately. In the following discussion, we will neglect these contributions. Also for the vector contributions, we only consider diagrams with top quarks coupling directly to photon. The diagrams with photon coupling to a bottom or light quarks and the top quark produced via gluon splitting are numerically small [112, 113]. Though the bottom triangle diagrams are needed and must be included to cancel the axial anomaly in the axial vector case [16, 31].

The first, second, and third terms on the RHS of Eq.(2) represent respectively the double-virtual, real-virtual, and double-real contributions. The double-virtual contributions contain explicit quadratic poles in ϵ , originating from loop corrections when the gluons are soft. Thanks to Bloch-Nordsieck and Kinoshita-Lee-Nauenberg theorem, the infrared divergences will be canceled by those in the real-virtual and double-real contributions. However, such cancellation is non-trivial because the infrared divergences in the real-virtual and double-real

contributions can only be made explicit *after* phase space integral. It is therefore necessary to perform the phase space integral in D dimension to regulate potential infrared divergences. This fact makes the calculation of real-virtual and double-real contributions difficult.

The singular region in the phase space is relatively simple for the real-virtual corrections, where the matrix elements are singular only when the energy of the final state gluon approaches zero. For the double-real contributions the singular region is much more involved. First, the matrix elements are singular in the double un-resolved region, where the energies of both the final state partons approach zero. Second, the matrix elements are also singular even in the single un-resolved region, where only one of the final state gluon is soft, or the final state massless partons become collinear. Fortunately, the singularities due to single un-resolved region is well understood, as they are the same one encounters in NLO QCD calculation. We therefore only need to deal with the double un-resolved region. To isolate the phase space singularities in this region, we introduce a phase-space slicing parameter τ , which is proportional to the total energy of QCD radiations in the final state, $\tau = 2(\sqrt{s} - (E_t + E_{\bar{t}}))/(\sqrt{s}(1 - 4m_t^2/s))$. Physically, when τ is non-zero, there is at least one massless parton in the final state with finite energy. We can divide the phase space into two slices using the theta function,

$$\sigma^{(2)} = \sigma_I^{(2)} + \sigma_{II}^{(2)}, \quad (4)$$

where $\sigma_I^{(2)} = \int d\sigma\theta(\delta_E - \tau)$ is the soft-virtual part, and $\sigma_{II}^{(2)} = \int d\sigma\theta(\tau - \delta_E)$ is the hard part, and δ_E is the cut-off parameter. There are still phase space singularities in both σ_I and σ_{II} . However, the phase space singularities in σ_{II} belong to the well understood one, because there is at most one massless parton in the final state whose energy can approach zero. We can therefore straight-forwardly calculate σ_{II} using any existing NLO infrared subtraction method. On the other hand, the soft-virtual part, σ_I , contains double un-resolved region, whose calculation needs additional efforts. An exact calculation for σ_I is difficult. However, if we choose δ_E to be small and ignore terms of $\mathcal{O}(\delta_E)$, we can calculate σ_I using matrix elements in the soft limit, and also expanding the phase space volume in the soft limit. Such approximation leads to enormous simplification and makes the analytical calculation feasible. We explain in detail the calculation of the soft-virtual part and hard part below.

2.1. The soft-virtual part

2.1.1. Factorization of the radiation-energy distribution

We can write the soft-virtual part as an integral over radiation-energy distribution,

$$\sigma_I^{(2)} = \int_0^{\delta_E} d\tau \frac{d\omega}{d\tau} \frac{d\sigma^{(2)}}{d\omega}, \quad (5)$$

where ω is twice the energy of final state QCD radiations, $\omega = 2(\sqrt{s} - E_t - E_{\bar{t}})$. The factor of 2 here is introduced by convention. Ignoring power suppressed terms in ω/m_t , we can write the distribution for $d\sigma/d\omega$ in small ω in a factorized form using the language of effective theory. $d\sigma^{(2)}/d\omega$ is simply the $\mathcal{O}(\alpha_s^2)$ corrections to this distribution. We start from the full distribution in QCD,

$$\frac{d\sigma}{d\omega} = \sum_{t, \bar{t}, X} (2\pi)^4 \delta^{(4)}(Q - p_t - p_{\bar{t}} - p_X) \delta(\omega - 2E(X)) L_{\mu\nu} \sum_{ij} \langle 0 | J_i^{\mu\dagger} | t\bar{t}X \rangle \langle t\bar{t}X | J_j^\nu | 0 \rangle, \quad (6)$$

where X denotes gluons and light quarks in the final state, and $E(X)$ denotes the energy of X . We do not include additional top-quark states in X because they give rise to finite corrections and can be incorporated into our numerical results separately in a simple way. The summation over final states in Eq. (6) becomes integral over D -dimensional phase space measure in dimensional regularization. For example, for two-gluon final state $X = gg$, we have

$$\sum_{t, \bar{t}, gg} (2\pi)^4 \delta^{(4)}(Q - p_t - p_{\bar{t}} - p_X) \xrightarrow{\text{dim.reg.}} \int d\Phi_{t\bar{t}, 2}, \quad (7)$$

where $d\Phi_{t\bar{t}, 2}$ is defined in Eq. (3). The lepton tensor includes only vector contributions from virtual photon exchange,

$$L_{\mu\nu} = -\frac{2e^2}{s} \left(g_{\mu\nu} - \frac{2(p_\mu^{e^+} p_\nu^{e^-} + p_\nu^{e^+} p_\mu^{e^-})}{s} \right), \quad (8)$$

where e is the QED coupling, and $p_\mu^{e^+}$ and $p_\mu^{e^-}$ are the four momentum of positron and electron. The production of top-quark pair via virtual photon exchange is described by two QCD currents,

$$J_1^\mu = -ieQ_t \bar{\Psi}(p_t) \gamma^\mu \Psi(p_{\bar{t}}), \quad J_2^\mu = \frac{eQ_t}{2m_t} \bar{\Psi}(p_t) \sigma^{\mu\nu} (p_t + p_{\bar{t}})_\nu \Psi(p_{\bar{t}}), \quad (9)$$

where $Q_t = 2/3$ is the electric charge number of top quark, and $\sigma^{\mu\nu} = \frac{i}{2}[\gamma^\mu, \gamma^\nu]$. Note that Eq. (6) is exact to leading order in electroweak interaction, and all orders in QCD interactions. It is also an exact distributions for ω . Calculation of Eq. (6) in perturbative QCD requires the calculation of both virtual corrections and phase space integral. Unfortunately, exact calculation of phase space integral is difficult beyond NLO. Certain approximation is needed in order to proceed. Since we are only interested in the energy distribution in the soft region, we can expand Eq. (6) to leading power in ω/m_t . Then the momentum conservation delta function factorizes as

$$\sum_{t, \bar{t}, X} (2\pi)^4 \delta^{(4)}(Q - p_t - p_{\bar{t}} - p_X) \simeq \sum_{t, \bar{t}} (2\pi)^4 \delta^{(4)}(Q - p_t - p_{\bar{t}}) \sum_X \quad (10)$$

in the region where $\Lambda_{QCD} \ll \omega \ll m_t$. The physics of such factorization is that as long as the energy of QCD radiations is small, they can hardly change the trajectory of heavy quark. The short-distance interaction which produces the top-quark pair can not resolve the activities of soft QCD radiations, therefore have tree-level like kinematics. We can describe the top quark and antitop quark by heavy quark fields $h_v(y)$ and $h_{\bar{v}}(y)$, labeled by the velocity of the heavy quarks, $p_t = m_t v$, $p_{\bar{t}} = m_t \bar{v}$. The QCD currents in Eq. (9) can then be matched to currents in Heavy Quark Effective Theory (HQET),

$$\mathcal{J}_1^\mu = -ieQ_t C_1(v, \bar{v}) \bar{h}_v \gamma^\mu h_{\bar{v}}, \quad \mathcal{J}_2^\mu = \frac{eQ_t}{2} C_2(v, \bar{v}) \bar{h}_v \sigma^{\mu\nu} (v + \bar{v})_\nu h_{\bar{v}}, \quad (11)$$

where the corresponding Wilson coefficients $C_1(v, \bar{v})$ and $C_2(v, \bar{v})$ can be obtained from the calculation of QCD form factor for heavy quark pair production. At leading power in HQET, the heavy quark field only interacts with gluons via eikonal interaction,

$$\mathcal{L}_{int} = \bar{h}_v(y) g v \cdot A_s(y) h_v(y) + \bar{h}_{\bar{v}}(y) g \bar{v} \cdot A_s(y) h_{\bar{v}}(y) \quad (12)$$

Such eikonal interactions can be absorbed into Wilson lines by a field redefinition [116],

$$(h_v(y))^\dagger = (h_v^{(0)}(y))^\dagger (Y_v(y))^\dagger, \quad h_{\bar{v}}(y) = Y_{\bar{v}}(y) h_{\bar{v}}^{(0)}(y), \quad (13)$$

where

$$\begin{aligned} (Y_v(y))^\dagger &= \mathbf{P} \exp \left(ig \int_0^\infty dz \cdot A(vz + y) \right) \\ Y_{\bar{v}}(y) &= \overline{\mathbf{P}} \exp \left(-ig \int_0^\infty dz \cdot A(\bar{v}z + y) \right) \end{aligned} \quad (14)$$

are the path-ordered and anti path-ordered Wilson lines. The decoupled heavy quark field $h_v^{(0)}(x)$ no longer interacts with gluon, but still annihilate the top quark field. The hadronic tensor now has a factorized form,

$$\begin{aligned} & \sum_X \delta(\omega - 2E(X)) \sum_{ij} \langle 0 | \mathcal{J}_i^{\mu\dagger} | t\bar{t}X \rangle \langle t\bar{t}X | \mathcal{J}_j^\nu | 0 \rangle \\ & = H^{\mu\nu} \sum_X \langle 0 | Y_v^\dagger Y_{\bar{v}} | X \rangle \delta(\omega - 2E(X)) \langle X | Y_{\bar{v}}^\dagger Y_v | 0 \rangle, \end{aligned} \quad (15)$$

where the summation is over all unrestricted massless final states. For example, for two-gluon final state with momentum p_1 and p_2 , we have

$$\sum_X \xrightarrow{\text{dim.reg.}} \int \frac{d^{D-1}p_1}{2E_1(2\pi)^{D-1}} \int \frac{d^{D-1}p_2}{2E_2(2\pi)^{D-1}} \quad (16)$$

$H^{\mu\nu}$ is the hard function,

$$H^{\mu\nu} = \sum_{i,j=1}^2 \langle 0 | \mathcal{J}_i^{(0),\mu\dagger} | t\bar{t} \rangle \langle t\bar{t} | \mathcal{J}_j^{(0),\nu} | 0 \rangle, \quad (17)$$

and $\mathcal{J}_i^{(0),\mu}$ is the decoupled HQET current, with $h_{v,\bar{v}}(y)$ replaced by $h_{v,\bar{v}}^{(0)}(y)$. Summing over the top quark spin and color ¹, the hard function can be evaluated explicitly,

$$H^{\mu\nu} = N_c \sum_{i,j=1}^2 C_i(v, \bar{v}) C_j^*(v, \bar{v}) h_{ij}^{\mu\nu}, \quad (18)$$

with

$$h_{11}^{\mu\nu} = e^2 Q_t^2 (-2sg^{\mu\nu} + 4(p_t^\mu p_{\bar{t}}^\nu + p_{\bar{t}}^\mu p_t^\nu)), \quad (19)$$

$$h_{12}^{\mu\nu} = h_{21}^{\mu\nu} = 2e^2 Q_t^2 (-sg^{\mu\nu} + (p_t^\mu + p_{\bar{t}}^\mu)(p_{\bar{t}}^\nu + p_t^\nu)), \quad (20)$$

$$h_{22}^{\mu\nu} = e^2 Q_t^2 \left(-2sg^{\mu\nu} + \left(2 - \frac{s}{2m_t^2} \right) (p_t^\mu p_{\bar{t}}^\nu + p_{\bar{t}}^\mu p_t^\nu) + \left(2 + \frac{s}{2m_t^2} \right) (p_t^\mu p_t^\nu + p_{\bar{t}}^\mu p_{\bar{t}}^\nu) \right) \quad (21)$$

$N_c = 3$ is the number of color in QCD. The matrix element of the Wilson lines defines the soft function for $t\bar{t}$ production,

$$S = \frac{1}{N_c} \sum_X \langle 0 | Y_v^\dagger Y_{\bar{v}} | X \rangle \delta(\omega - 2E(X)) \langle X | Y_{\bar{v}}^\dagger Y_v | 0 \rangle, \quad (22)$$

¹ It should be noted that our formalism also allows full spin dependence for heavy quark, since the eikonal approximation preserves spin.

The summation is over all possible QCD final states. We have chosen the normalization such that at LO the soft function is $\delta(\omega)$. The calculation for soft function is much easier than the exact phase space integral, thanks to the eikonal approximation.

We can now write down a factorized formula for the radiation-energy distribution in top-quark pair production,

$$\frac{d\sigma_{\text{s.v.}}}{d\omega} = \frac{1}{8s} \int \frac{d^3 p_t}{2E_t(2\pi)^3} \int \frac{d^3 p_{\bar{t}}}{2E_{\bar{t}}(2\pi)^3} (2\pi)^4 \delta^{(4)}(Q - p_t - p_{\bar{t}}) L_{\mu\nu} H^{\mu\nu} S(x, \omega) , \quad (23)$$

where we have also included the initial state flux and spin average factor. The variable x is defined as

$$x = \frac{1 - \sqrt{1 - \frac{4m_t^2}{s}}}{1 + \sqrt{1 - \frac{4m_t^2}{s}}} \quad (24)$$

For fixed m_t , $x \rightarrow 0$ is the high energy limit, while $x \rightarrow 1$ is the threshold limit. Eq. (23) is only valid at leading power in ω . The soft function is fully differential in the top and antitop momentum, but inclusive in the QCD radiations. This is not a problem as we will use this formula only in the limit of small ω , where the QCD radiations can not be resolved by any reasonable experimental measurement.

The phase space integral in Eq. (23) becomes trivial. Integrating out the azimuthal angle dependence of top quark, we obtain

$$\frac{d^2 \sigma_{\text{s.v.}}}{d\omega d \cos \theta_t} = \mathcal{H}(\cos \theta_t, m_t, s) S(x, \omega) , \quad (25)$$

where

$$\begin{aligned} \mathcal{H}(\cos \theta_t, m_t, s) &= \frac{1}{8s} \int \frac{d^3 p_t}{2E_t(2\pi)^3} \int \frac{d^3 p_{\bar{t}}}{2E_{\bar{t}}(2\pi)^3} \\ &\times (2\pi)^4 \delta^{(4)}(Q - p_t - p_{\bar{t}}) \delta \left(\cos \theta_t - \frac{\mathbf{p}_t \cdot \mathbf{p}_e}{|\mathbf{p}_t| |\mathbf{p}_e|} \right) L_{\mu\nu} H^{\mu\nu} \end{aligned} \quad (26)$$

The soft function is a distribution in ω . It is often convenient to perform a Laplace transformation,

$$\begin{aligned} \frac{d^2 \tilde{\sigma}_{\text{s.v.}}}{d\kappa d \cos \theta_t} &= \int_0^\infty d\omega \exp \left(-\frac{\omega}{e^{\gamma_E \kappa}} \right) \frac{d^2 \sigma_{\text{s.v.}}}{d\omega d \cos \theta_t} \\ &\equiv \mathcal{H}(\cos \theta_t, m_t, s) \tilde{s}(x, L_\kappa) , \end{aligned} \quad (27)$$

where $L_\kappa = \ln(\kappa/\mu)$. The renormalized soft function depends on κ only through terms of the form L_κ^n , where n is a positive integer. It is therefore possible to invert the Laplace transformation in close form [117],

$$\frac{d^2\sigma_{\text{s.v.}}}{d\tau d\cos\theta_t} = \mathcal{H}(\cos\theta_t, m_t, s) \lim_{\eta \rightarrow 0} \left[\tilde{s}(x, \partial_\eta) \left(\frac{\sqrt{s}(1 - 4m_t^2/s)}{\mu} \right)^\eta \frac{1}{\tau^{1-\eta}} \frac{\exp(-\gamma_E\eta)}{\Gamma(\eta)} \right], \quad (28)$$

where we recall that $\tau = \omega/(\sqrt{s}(1 - 4m_t^2/s))$. Eq. (28) is interpreted as first expanding in η as a Taylor series within the square bracket, using the well-known plus-distribution expansion

$$\frac{1}{\tau^{1-\eta}} = \frac{\delta(\tau)}{\eta} + \frac{1}{[\tau]_+} + \eta \left[\frac{\ln \tau}{\tau} \right]_+ + \mathcal{O}(\eta^2), \quad (29)$$

then taking the $\eta \rightarrow 0$ limit.

2.1.2. Hard function from QCD heavy quark form factor

The Wilson coefficients defined in Eq. (11) can be obtained from the QCD heavy quark form factor. The latter has been computed for the vector contributions, axial contributions, and anomaly contributions by Bernreuther et.al [29–31]. The vector contributions have been computed independently later in ref. [32], confirming previous results.

In ref. [29], the vector contributions to heavy quark form factor are given to two loops in QCD. The results are expressed in terms of two dimensionless scalar form factors, $\hat{F}_1(x)$ and $\hat{F}_2(x)$,

$$-ieQ_t\bar{u}(p_t) \left(\hat{F}_1(x)\gamma^\mu + \frac{1}{2m_t}\hat{F}_2(x)i\sigma^{\mu\nu}(p_\nu^t + p_\nu^{\bar{t}}) \right) v(p_{\bar{t}}) \quad (30)$$

Here the scalar form factors are related to those computed in Eq. (57) and (58) of ref. [29] by an additional renormalization,

$$\hat{F}_i(x, \alpha_s^{N_l}) = F_i(x, \alpha_s^{N_f}(\alpha_s^{N_l})), \quad i = 1, 2, \quad (31)$$

where

$$\alpha_s^{N_f}(\alpha_s^{N_l}) = \alpha_s^{N_l} \left[1 + \frac{8}{3}T_R N_h \frac{\alpha_s^{N_l}}{4\pi} \left(-\frac{1}{2}L_H + \epsilon \left(\frac{L_H^2}{4} + \frac{1}{24}\pi^2 \right) \right) + \frac{\epsilon}{12} \left(\frac{\alpha_s^{N_l}}{4\pi} \right) \beta_0^{(N_f)}\pi^2 \right], \quad (32)$$

with $N_f = N_l + N_h$. $N_l = 5$ is the number of light quark flavor, and $N_h = 1$ is the number of heavy quark flavor. $T_R = 1/2$ in QCD, $L_H = \ln(m_t^2/\mu^2)$. The QCD beta function for N_f

quark flavor is given by

$$\beta_0^{(N_f)} = \frac{11}{3}C_A - \frac{4}{3}T_R(N_l + N_h) \quad (33)$$

where $C_A = 3$ in QCD. Unless otherwise specified, we will denote $\alpha_s^{N_l}$ as α_s below. Note that $\hat{F}_i(x)$ and $F_i(x)$ only differ starting from two loops. The origin for such difference is that in ref. [29], the renormalization of strong coupling is performed in $\overline{\text{MS}}$ scheme, running with N_f flavors. Also the authors of ref. [29] include a factor $\Gamma(1 + \epsilon) \exp(\epsilon\gamma_E)$ in the coupling renormalization, where $\Gamma(z)$ is Euler's Gamma function, and $\gamma_E = 0.577216\dots$. However, we choose to perform the calculation with α_s running with N_l flavors, and also without the additional factor $\Gamma(1 + \epsilon) \exp(\epsilon\gamma_E)$. The decoupling of heavy quark flavor is realized by the second term on the RHS of Eq. (32) [118–121], while the third factor gets rid of the additional factor $\Gamma(1 + \epsilon) \exp(\epsilon\gamma_E)$ through to $\mathcal{O}(\alpha_s^2)$ [122].

The scalar form factors are functions of x . Writing them as an expansion in $a_s = \alpha_s(\mu)/(4\pi)$,

$$\hat{F}_i(x) = \hat{F}_i^{(0l)}(x) + a_s \hat{F}_i^{(1l)}(x) + a_s^2 \hat{F}_i^{(2l)}(x) + \mathcal{O}(a_s^3) , \quad (34)$$

we have at LO in QCD

$$\hat{F}_1^{(0l)}(x) = 1, \quad \hat{F}_2^{(0l)}(x) = 0 \quad (35)$$

Using the additional renormalization relation in Eq. (31), the one-loop and two-loop form factors can be read off from ref. [29]. These form factors are UV finite but IR divergent. To calculate the Wilson coefficients defined in Eq. (11), one needs to calculate the form factors in the effective theory. The Wilson coefficients are simply the differences of the form factor in QCD and the form factor in effective theory. In dimensional regularization with external state onshell, the form factors in the effective theory at one loop and beyond vanish because they involve only scaleless integral. Since the IR divergences in the QCD calculation and effective theory calculation must match, it implies that the UV divergences in the effective theory calculation are exactly the negative of the IR divergence in the QCD calculation. Therefore, renormalization of the UV divergences in the effective theory is simply amount to performing an IR subtraction to the form factor in QCD,

$$C_i(x) = \lim_{\epsilon \rightarrow 0} \left[Z_{H,i} \hat{F}_i(x) \right] , \quad i = 1, 2 , \quad (36)$$

where the IR subtraction factor is defined such that $C_i(x)$ is order by order finite, i.e., $Z_{H,i}$ absorbs *only* the ϵ poles in $\hat{F}_i(x)$. For the convenience of reader, we give below the explicit expression for $C_i(x)$ at one loop, as derived from the QCD form factors in ref. [29]. We have checked that using ref. [32], we get the same Wilson coefficients.

The one-loop Wilson coefficients are

$$\begin{aligned}
C_1^{(1l)}(x) = & C_F \left[L_H \left(\left(\frac{2}{x+1} - \frac{2}{x-1} - 2 \right) H(0, x) + 2 \right) + \left(-\frac{4}{x+1} + \frac{2}{x-1} + 3 \right) H(0, x) \right. \\
& + \left(-\frac{2}{x+1} + \frac{2}{x-1} + 2 \right) H(0, 0, x) + \left(-\frac{4}{x+1} + \frac{4}{x-1} + 4 \right) H(1, 0, x) \\
& \left. - \frac{8\zeta_2}{x-1} + \frac{8\zeta_2}{x+1} - 4(2\zeta_2 + 1) \right] + i\pi C_F \left[L_H \left(\frac{2}{x+1} - \frac{2}{x-1} - 2 \right) \right. \\
& + \left(-\frac{2}{x+1} + \frac{2}{x-1} + 2 \right) H(0, x) + \left(-\frac{4}{x+1} + \frac{4}{x-1} + 4 \right) H(1, x) \\
& \left. + \frac{2}{x-1} - \frac{4}{x+1} + 3 \right] \tag{37}
\end{aligned}$$

$$C_2^{(1l)}(x) = 2C_F \left(-\frac{1}{x-1} - \frac{1}{x+1} \right) (H(0, x) + i\pi) , \tag{38}$$

where $C_F = 4/3$ in QCD. The imaginary part in the Wilson coefficients results from analytical continuation of the form factors from spacelike to timelike kinematics. The function $H(\vec{w}, x)$ is harmonic polylogarithm (HPL) introduced in ref. [123]. We use `hplog` [124] for the numerical calculation of HPLs in this work. The `Mathematica` file for the two-loop Wilson coefficients can be found in the arXiv submission of this paper.

2.1.3. Perturbative expansion of the radiation-energy distribution through to NNLO

To expand the equation for radiation-energy distribution in Eq. (28) in α_s , we also need the soft function to NNLO, which have been computed only recently [125]. The Laplace transformed soft function has the generic form

$$\begin{aligned}
\tilde{s}(x, L_\kappa) = & 1 + a_s \left(L_\kappa \gamma_0^s(x) + c_1(x) \right) + a_s^2 \left[L_\kappa^2 \left(\frac{1}{2} \left(\gamma_0^s(x) \right)^2 - \beta_0 \gamma_0^s(x) \right) \right. \\
& \left. + L_\kappa \left(c_1(x) \left(\gamma_0^s(x) - 2\beta_0 \right) + \gamma_1^s(x) \right) + c_2(x) \right] + \mathcal{O}(a_s^3) . \tag{39}
\end{aligned}$$

through to $\mathcal{O}(\alpha_s^2)$, where β_0 is the LO QCD beta function with N_l light flavor only,

$$\beta_0 = \frac{11}{3}C_A - \frac{4}{3}T_R N_l , \tag{40}$$

and $\gamma_0^s(x)$ and $\gamma_1^s(x)$ are the well-known cusp anomalous dimension [126–128]. We reproduce them here for the sake of completeness

$$\gamma_0^s(x) = -8C_F \left[1 + \frac{1+x^2}{1-x^2} H(0, x) \right] \quad (41)$$

$$\gamma_1^s(x) = \frac{160}{9} C_F N_l T_R \left[1 + \frac{1+x^2}{1-x^2} H(0, x) \right] \quad (42)$$

$$\begin{aligned} &+ C_A C_F \left[-\frac{392}{9} + 16\zeta_2 \frac{1+9x^2}{1-x^2} + 16 \frac{(1+x^2)^2}{(1-x^2)^2} \left(2H(0, x) \left(H(0, -1, x) - H(0, 1, x) \right) \right. \right. \\ &- 4H(0, 0, -1, x) + 4H(0, 0, 1, x) - \zeta(3) \left. \left. + 32 \frac{1+x^2}{1-x^2} \left(H(0, x) \left(H(-1, x) - H(1, x) - \frac{67}{36} \right) \right. \right. \right. \\ &- \left. \left. H(0, -1, x) + H(0, 1, x) \right) \right] - \frac{32}{3} \frac{x^2(1+x^2)}{(1-x^2)^2} H^3(0, x) - \frac{32x^2}{1-x^2} H^2(0, x) \\ &+ 16\zeta_2 \frac{(1+x^2)(1+9x^2)}{(1-x^2)^2} H(0, x) \left. \right]. \end{aligned}$$

The soft function is largely fixed by the renormalization group equation it obeys [126]. The genuine two-loop corrections to the soft function are summarized by the scalar function $c_2(x)$, which is first computed in ref. [125]². With all these results at hand, we can write down the radiation-energy distribution through to NNLO, up to power-correction terms in τ . Writing $\mathcal{H}(\cos \theta_t, m_t, s)$ as an expansion in a_s , $\mathcal{H}(\cos \theta_t, m_t, s) = \mathcal{H}_0 + a_s \mathcal{H}_1 + a_s^2 \mathcal{H}_2 + \dots$, the results are

$$\frac{d^2 \sigma_{\text{s.v.}}^{(1l)}}{d\tau d \cos \theta_t} = [(c_1(x) + L_H \gamma_0^s) \mathcal{H}_0 + \mathcal{H}_1] \delta(\tau) + 2\gamma_1^s(x) \mathcal{H}_0 \frac{1}{[\tau]_+} \quad (43)$$

$$\begin{aligned} \frac{d^2 \sigma_{\text{s.v.}}^{(2l)}}{d\tau d \cos \theta_t} &= \left[\frac{1}{2} \mathcal{H}_0 L_H^2 \gamma_0^s (\gamma_0^s - \beta_0) + L_H (\mathcal{H}_0 (c_1(x) \gamma_0^s - \beta_0 c_1(x) + \gamma_1^s) + \mathcal{H}_1 \gamma_0^s) \right. \\ &+ \mathcal{H}_0 \left(c_2(x) + \frac{1}{3} \pi^2 \beta_0 \gamma_0^s - \frac{1}{3} \pi^2 (\gamma_0^s)^2 \right) + \mathcal{H}_1 c_1(x) + \mathcal{H}_2 \left. \right] \delta(\tau) \\ &+ \left[\mathcal{H}_0 L_H (2(\gamma_0^s)^2 + \mathcal{H}_0 (2c_1(x) \gamma_0^s - 2\beta_0 c_1(x) + 2\gamma_1^s) - 2\beta_0 \gamma_0^s) + 2\mathcal{H}_1 \gamma_0^s \right] \frac{1}{[\tau]_+} \\ &- 4\mathcal{H}_0 \gamma_0^s (\beta_0 - \gamma_0^s) \left[\frac{\ln \tau}{\tau} \right]_+ \quad (44) \end{aligned}$$

This is the main results for the soft-virtual part.

² Note that results presented in ref. [125] are given in terms of generalized polylogarithms, $G(\dots; x)$, with weight alphabet drawn from $\{-1, 0, 1\}$. They are related to HPLs by a simple relation, $G(\vec{w}; x) = (-1)^{n_1} H(\vec{w}, x)$, where n_1 is the number of occurrence of alphabet 1 in the weight vector \vec{w} .

2.2. The hard part

The hard part $\sigma_{II}^{(2)}$ consists of the real-virtual corrections, $e^+e^- \rightarrow t\bar{t}g$ at one loop, and the double-real corrections, $e^+e^- \rightarrow t\bar{t}gg(q\bar{q})$ at tree level. As mentioned above, the infrared divergences in this part only involve single unresolved limit, thus can be extracted using standard NLO subtraction technique. In this paper we employ the massive version of dipole subtraction method [129]. The one-loop real-virtual calculation is carried out by the automated program `GoSam2.0` [130] with loop integral reductions from `Ninja` [131, 132] and scalar integrals from `OneL0op` [133, 134]. Since $\sigma_{II}^{(2)}$ is IR finite, it can be compared directly to the NLO QCD calculation of $e^+e^- \rightarrow Q\bar{Q}g$, *e.g.*, ref. [25], and shows very good agreements.

Once the soft-virtual part and hard part are known, the full corrections are simply the sum of them. The soft-virtual part has born kinematics in the final state, since the QCD radiations are soft and have been integrated out. Its numerical implementation is therefore trivial. The hard part is nothing but the usual NLO QCD corrections to the process $e^+e^- \rightarrow t\bar{t}g$, as described above. We believe this is the most important advantage of phase-space slicing method, because its numerical implementation is no more difficult than a typical NLO calculation.

However, the drawback of phase-slicing method is also clear. In principle, the sum of the soft-virtual part and hard part is independent of the arbitrary cut-off parameter δ_E in the limit of $\delta_E \rightarrow 0$. Furthermore, since we will approximate the kinematics of the soft part as born kinematics in our numerical calculation, δ_E needs to be small for such approximation to hold. In realistic calculation, such a limit can never be reached in the hard part. Nevertheless, our formalism is exact in the hard part, and include all the leading singular dependence of δ_E in the soft-virtual part, such that the sum only depends mildly on δ_E . To estimate the form of the subleading term missing in the soft-virtual part, we note that an exact τ distribution in small τ should have the following form

$$\frac{d\sigma^{(2)}}{d\tau} = A(x) \left[\frac{\ln \tau}{\tau} \right]_+ + \frac{B(x)}{[\tau]_+} + C(x)\delta(\tau) + D(x) \ln \tau + \text{subleading terms} \quad (45)$$

Our calculation includes exact results for the first three coefficients, $A(x)$, $B(x)$ and $C(x)$, but not $D(x)$. Integrating over the fourth term over τ gives

$$D(x) \int_0^{\delta_E} d\tau \ln \tau \simeq D(x)\delta_E \ln \delta_E + \text{subleading terms in } \tau \quad (46)$$

We therefore expect the leading missing δ_E dependence in the sum of the soft-virtual part and hard part is proportional to $\delta_E \ln \delta_E$ at NNLO. To minimize the impact of such contributions, we have to choose very small cut-off parameter δ_E . This is not a problem for the soft-virtual part, as δ_E dependence there is analytical. For the hard part, choosing extremely small δ_E leads to finite but very large corrections, comparing to the corrections to the sum. Thus there has to be delicate cancellation of large corrections between the soft-virtual part and hard part. A possible improvement would be including also the subleading terms $D(x) \ln \tau$ in the calculation. Such “next-to-eikonal corrections” have been considered before in Drell-Yan production through to NNLO [135, 136]. It would be interesting to calculate $D(x)$ along the same line.

3. Numerical results

We present our numeric results in this section. As mentioned before, we use two-loop running of the QCD coupling constants with $N_l = 5$ active quark flavors and $\alpha_s(M_Z) = 0.118$. We choose the G_F parametrization scheme [138] for the EW couplings with $M_W = 80.385$ GeV, $M_Z = 91.1876$ GeV, $M_t = 173$ GeV, and $G_F = 1.166379 \times 10^{-5}$ GeV⁻² [139]. The renormalization scale is set to the center of mass energy \sqrt{s} unless otherwise specified.

The production cross sections due to virtual photon exchange through to NNLO in QCD can be expressed as

$$\sigma_{NNLO,\gamma} = \sigma_{LO,\gamma} (1 + \Delta^{(1),\gamma} + \Delta^{(2),\gamma}), \quad (47)$$

where $\Delta^{(1,2),\gamma}$ denote respectively the $\mathcal{O}(\alpha_s)$ and $\mathcal{O}(\alpha_s^2)$ QCD corrections. The $\mathcal{O}(\alpha_s^2)$ corrections $\Delta^{(2),\gamma}$ can be further decomposed according to color factors, i.e., the Abelian contributions, the non-Abelian contributions, the light-fermionic contributions, and the heavy-fermionic contributions. Alternative notation used in [8, 16, 17] follows

$$\sigma_{NNLO,\gamma} = \sigma_{\mu^+\mu^-, \gamma} \left(R^{(0)} + \frac{\alpha_s(\mu^2)}{\pi} C_F R^{(1)} + \left(\frac{\alpha_s(\mu^2)}{\pi} \right)^2 R^{(2)} \right), \quad (48)$$

with $\sigma_{\mu^+\mu^-, \gamma}$ be the cross section of muon pair production, and

$$R^{(2)} = C_F^2 R_A^{(2)} + C_A C_F R_{NA}^{(2)} + C_F T_R N_l R_{lF}^{(2)} + C_F T_R R_{hF}^{(2)}, \quad (49)$$

depends only on $r = 2m_t/\sqrt{s}$. The four contributions in Eq. (49) are denoted by “ C_F ”, “ C_A ”, “ N_l ”, and “ N_h ” respectively in the following figures and discussions. Analytical

results for $R^{(2)}$ are presented for production near threshold [8, 9] or in the high-energy expansions [16, 17] with which we compare our numerical results. Note that for the $\mathcal{O}(\alpha_s^2)$ results on inclusive cross sections or $R^{(2)}$ in below we include the real corrections with four top-quark final states, which are also present in above calculations of high-energy expansions. We do not include those four-top contributions in the differential distributions since they could be measured separately.

3.1. Inclusive cross sections

As usual in phase-space slicing method, $\Delta^{(2),\gamma}$ depends only weakly on the cut-off parameter δ_E and approaches the genuine $\mathcal{O}(\alpha_s^2)$ corrections when δ_E is small enough. Fig. 1 shows $\Delta^{(2),\gamma}$ as functions of δ_E for different collision energies. For each of the energy choices, $\Delta^{(2),\gamma}$ receives contributions from below the cut-off $\Delta_1^{(2),\gamma}$ (soft-virtual part), and above the cut-off $\Delta_{2/3}^{(2),\gamma}$ (hard parts). Each of the three parts depends strongly on δ_E with variations as large as 30% for example for $\sqrt{s} = 500$ GeV. However, their sum, $\Delta^{(2),\gamma}$ remains almost unchanged when δ_E varies between 10^{-2} and 10^{-4} as demonstrated in Fig. 1. For production near the threshold, e.g., $\sqrt{s} = 350$ GeV, the dominant contribution to the $\mathcal{O}(\alpha_s^2)$ corrections is from the two-loop virtual corrections as included in $\Delta_1^{(2),\gamma}$. The remaining dependences of $\Delta^{(2),\gamma}$ on δ_E are further plotted in Fig. 2. Here in $\delta\Delta^{(2),\gamma}$ we have subtracted the high energy expansion results [16, 17] from our numerical results for comparison. The solid lines are scattering plots and the dashed lines are fitted curves assuming $\delta\Delta^{(2),\gamma} = f_0 + f_1\delta_E \ln \delta_E + f_2\delta_E$, where f_i are constants independent of δ_E . The fitted coefficients are $f_{0,1,2} = \{0.4555, -0.00025, 0.0037\}$, $\{0.00005, -0.0050, 0.044\}$, and $\{-0.00003, 0.016, 0.066\}$ for the three collision energies respectively. Note that the f_0 term represents difference of our numerical results in the limit of $\delta_E \rightarrow 0$ (genuine $\mathcal{O}(\alpha_s^2)$ corrections) with the high energy expansion results. f_1 and f_2 terms are the systematic errors due to finite δ_E choices. Assuming $\delta_E = 2 \times 10^{-4}$, the f_1 and f_2 terms are estimated to be less than 10^{-4} for above collision energies. Thus choosing $\delta_E = 2 \times 10^{-4}$ should be sufficient for a realistic calculation. The smallness of f_0 for $\sqrt{s} = 500$ and 1000 GeV indicates a very good agreements of our numerical results with the high energy expansion ones.

Fig. 3 shows detailed comparison of our numerical results with the threshold [8, 9] and high-energy expansion results [16, 17] in a wide range of energy. The cut-off parameter is

chosen as $\delta_E = 2 \times 10^{-4}$. We present the comparisons both for the $\mathcal{O}(\alpha_s^2)$ corrections as well as their ratios. It can be seen that our full results works well in the entire energy region considered, i.e., approaching the threshold results for lower energies and the high-energy expansions on the other end. However, one may notice the differences between the high-energy expansion results and ours for $\sqrt{s} > 1000$ GeV in the ratio plot. The differences are due to the power corrections we mentioned earlier. For $\sqrt{s} > 1000$ GeV, the $\mathcal{O}(\alpha_s^2)$ corrections are at per mile level as a result of large cancellation between soft-virtual part and hard part. However, no such large cancellation exist for the power correction terms. This is because we are only neglecting power correction terms in soft-virtual part, not in hard part. Therefore, in general the power corrections are proportional to the LO cross sections and depend on threshold behaviors of $d\sigma^{(2)}/d\tau$ as shown in Eq. (45). Furthermore, the power corrections contain logarithmic terms of the form $\ln(s/m_t^2)$, which become large as s increased. For $\sqrt{s} < 1000$ GeV, which is the energy range phenomenologically important, the power corrections are negligibly small for the chosen cut-off parameter and our results are accurate. For $\sqrt{s} > 1000$ GeV, power corrections become important and a smaller cut-off parameter is needed to suppress them. That requires much more CPU times in order to control the MC integration errors which is not worth considering the smallness of the absolute corrections.

Further comparisons for the ratios are presented in Figs. 4-5 as functions of r for different color structures. The left end of each plot, with $r \sim 0.17$, corresponds to a collision energy of 2 TeV. Besides the high-energy and threshold expansions, we also include into comparison results from Padé approximation for which the analytical expressions are available for Abelian $R_A^{(2)}$ and non-Abelian $R_{NA}^{(2)}$ pieces in Ref. [137]. The Padé approximation is an interpolation based on the existed results in different limits and works for the entire energy range. Again we can see good agreement of our results with the high-energy and threshold expansions in the corresponding limit, and also the Padé approximation in the entire energy region for $r > 0.4$. The kinks in the Abelian contributions are due the fact that $R^{(2)}$ crosses zero at that point. The deviation of our results for $r < 0.4$ again are due to the power corrections. It is understood that the power corrections are different for different color structures. Especially, they are negligible for “ N_h ” part since there is no logarithmic enhancement as seen in Eq. (44). We have checked that if we choose larger or smaller values of δ_E , our curves do get farther or closer to the high-energy expansion or Padé approxima-

tion curves for $r < 0.4$. The small differences between the Padé approximation [137] and high-energy expansion results [16, 17] are due to that the former one is based on expansion with less terms in m^2/s .

We further show reduction of the scale variations by including the $\mathcal{O}(\alpha_s^2)$ corrections in Fig. 6. We vary the renormalization scale μ_r around the nominal choice $\mu_r = \sqrt{s}$ by a factor of 10 downward and 4 upward. The scale dependence have been reduced significantly for $\sqrt{s} = 500$ and 1000 GeV, e.g., from 6% at the NLO to 1% at the NNLO for a collision energy of 500 GeV. The NNLO results still show a large scale dependence near production threshold due to the large corrections and require resummations for further improvements.

3.2. Differential distributions

We can calculate fully differential distributions up to NNLO in QCD based on the phase-space slicing method. At LO, there is only one non-trivial kinematic variable, which we can choose either as cosine of the scattering angle between the final-state top quark and the initial-state electron $\cos\theta_t$, or transverse momentum of the top quark with respect to the beam $p_{T,t}$. Similar as the inclusive cross section, we can define the $\mathcal{O}(\alpha_s)$ and $\mathcal{O}(\alpha_s^2)$ corrections for each kinematic bin, $\Delta_{bin}^{(1),\gamma}$ and $\Delta_{bin}^{(2),\gamma}$, in analogy to Eq. (47). The results are shown in Fig. 7 for $\cos\theta_t$ and 8 for $p_{T,t}$ distributions with collision energies of 350, 500, and 1000 GeV. For each of them we plot the $\mathcal{O}(\alpha_s^2)$ corrections with two different δ_E choices, 10^{-3} and 5×10^{-4} . By comparing those two results we can see very good stabilities of the $\mathcal{O}(\alpha_s^2)$ distributions for δ_E small enough \sim a few 10^{-4} , similar as the inclusive cross sections.

As can be seen from Fig. 7, both the $\mathcal{O}(\alpha_s)$ and $\mathcal{O}(\alpha_s^2)$ corrections are flat for $\sqrt{s} = 350$ GeV where they are dominated by virtual corrections. The $\cos\theta_t$ distribution is symmetric in forward and backward region for pure photon contributions. For $\sqrt{s} = 500$ GeV, the $\mathcal{O}(\alpha_s^2)$ corrections are slightly larger in region of $|\cos\theta_t| \sim 1$ than central region, and are about 13% of the $\mathcal{O}(\alpha_s)$ corrections in size. The $\mathcal{O}(\alpha_s^2)$ corrections for $\cos\theta_t$ distribution are totally negligible comparing to the $\mathcal{O}(\alpha_s)$ ones for $\sqrt{s} = 1000$ GeV.

The transverse momentum distributions in Fig. 8 show a different feature comparing to the angular distribution since they are also affected by the energy spectrum of the top quark. The real corrections pull the energy spectrum to the lower end and thus the $p_{T,t}$ distribution as well. As shown in Fig. 8, both the $\mathcal{O}(\alpha_s)$ and $\mathcal{O}(\alpha_s^2)$ corrections start as positive in low

p_T and then decrease to negative values near the kinematic limits. The $\mathcal{O}(\alpha_s^2)$ corrections show a relatively larger impact in the $p_{T,t}$ distribution.

Besides, we can also investigate distributions like, $\Delta\phi_{t\bar{t}}$, difference of azimuthal angles of top and antitop quark, and their invariant mass, $m_{t\bar{t}}$. Since they are both a delta function at the LO, our $\mathcal{O}(\alpha_s^2)$ corrections are effectively NLO for those observables. We plot the LO distributions together with the $\mathcal{O}(\alpha_s)$ and $\mathcal{O}(\alpha_s^2)$ corrections in Fig. 9. The corrections have been rescaled for comparison. For bins with vanishing cross sections at the LO, we have compared our $\mathcal{O}(\alpha_s)$ and $\mathcal{O}(\alpha_s^2)$ corrections with the calculations of $Q\bar{Q} + jet$ production up to NLO in [25] and found very good agreement.

4. Conclusion

To conclude, we have presented a fully differential NNLO QCD calculation for the photon exchange contributions to electroweak top quark pairs production at e^+e^- colliders. Our calculations are based on a NNLO generalization of the phase-space slicing method. Similar methods were introduced some time ago to compute the N_l -dependent contributions to the total cross section [114, 115]. To the best of our knowledge, the results presented in this paper for the rest of the color structures are new. Let us emphasize that we present various differential distributions as well at NNLO for the first time. Whenever possible, we have compared our results to existing analytical calculations. We find complete agreement with the known results, both in the threshold [8–11] and in the high-energy regimes [13–17]. Although their calculation was beyond the scope of this work, the Z exchange contributions can be straightforwardly derived using the phase-space slicing technique discussed in this paper. The Z exchange contributions are of fundamental phenomenological importance and will be treated in a future publication.

Inspired by the successful application of q_T subtraction method of Catani and Grazzini [72], recently there has been some interest and progress in applying the phase-space slicing method to NNLO QCD calculations. For instance, top quark decay [99], Drell-Yan production [140], and Higgs production [141] have all been studied in schemes very similar to the one described in this work. This paper demonstrates that phase-space slicing can also be used to calculate top quark production processes, albeit at e^+e^- colliders. Our calculation shows that fully differential NNLO corrections in e^+e^- annihilation are not much harder to

obtain than typical NLO corrections to QCD processes once a good IR-safe observable has been defined and the corresponding hard and soft functions are known. In future work, it would be interesting to apply the phase-space slicing method to other NNLO QCD calculations relevant to the physics of future linear colliders and to generalize the method to allow for the treatment of parton-initiated processes.

ACKNOWLEDGMENTS

We are grateful to A. Hoang and T. Tuebner for sharing their results for the light quark contributions to the soft-virtual part of our calculation in the small mass regularization scheme for comparison. We thank P. Nason and C. Oleari for providing us with the numerical program used to perform the analysis discussed in ref. [25]. We are particularly indebted to R. M. Schabinger for numerous helpful discussions, and detailed feedback on the manuscript. We would also like to thank V. Hirschi for helpful discussions and to Y. Li for useful comments on the paper. J.G. was supported by the U.S. DOE Early Career Research Award DE-SC0003870 and by the Lightner-Sams Foundation. H.X.Z. was supported by the U.S. DOE under contract DEAC0276SF00515, and by the Munich Institute for Astro- and Particle Physics (MIAPP) of the DFG cluster of excellence “Origin and Structure of the Universe”.

-
- [1] S. Schael *et al.* [ALEPH and DELPHI and L3 and OPAL and SLD and LEP Electroweak Working Group and SLD Electroweak Group and SLD Heavy Flavour Group Collaborations], Phys. Rept. **427**, 257 (2006) [hep-ex/0509008].
 - [2] E. Devetak, A. Nomerotski and M. Peskin, Phys. Rev. D **84**, 034029 (2011) [arXiv:1005.1756 [hep-ex]].
 - [3] J. Jersak, E. Laermann and P. M. Zerwas, Phys. Rev. D **25**, 1218 (1982) [Erratum-ibid. D **36**, 310 (1987)].
 - [4] W. Beenakker, S. C. van der Marck and W. Hollik, Nucl. Phys. B **365**, 24 (1991).
 - [5] C. R. Schmidt, Phys. Rev. D **54**, 3250 (1996) [hep-ph/9504434].
 - [6] J. Kodaira, T. Nasuno and S. J. Parke, Phys. Rev. D **59**, 014023 (1998) [hep-ph/9807209].

- [7] H. X. Liu, C. S. Li and Z. J. Xiao, Phys. Lett. B **458**, 393 (1999) [hep-ph/9901205].
- [8] A. Czarnecki and K. Melnikov, Phys. Rev. Lett. **80**, 2531 (1998) [hep-ph/9712222].
- [9] M. Beneke, A. Signer and V. A. Smirnov, Phys. Rev. Lett. **80**, 2535 (1998) [hep-ph/9712302].
- [10] A. H. Hoang and T. Teubner, Phys. Rev. D **58**, 114023 (1998) [hep-ph/9801397].
- [11] A. H. Hoang, M. Beneke, K. Melnikov, T. Nagano, A. Ota, A. A. Penin, A. A. Pivovarov and A. Signer *et al.*, Eur. Phys. J. direct C **2**, 1 (2000) [hep-ph/0001286].
- [12] S. J. Brodsky, A. H. Hoang, J. H. Kuhn and T. Teubner, Phys. Lett. B **359**, 355 (1995) [hep-ph/9508274].
- [13] S. G. Gorishnii, A. L. Kataev and S. A. Larin, Nuovo Cim. A **92**, 119 (1986).
- [14] K. G. Chetyrkin and J. H. Kuhn, Phys. Lett. B **248**, 359 (1990).
- [15] K. G. Chetyrkin and J. H. Kuhn, Nucl. Phys. B **432**, 337 (1994) [hep-ph/9406299].
- [16] R. Harlander and M. Steinhauser, Eur. Phys. J. C **2**, 151 (1998) [hep-ph/9710413].
- [17] K. G. Chetyrkin, R. Harlander, J. H. Kuhn and M. Steinhauser, Nucl. Phys. B **503**, 339 (1997) [hep-ph/9704222].
- [18] G. Altarelli and B. Lampe, Nucl. Phys. B **391**, 3 (1993).
- [19] V. Ravindran and W. L. van Neerven, Phys. Lett. B **445**, 214 (1998) [hep-ph/9809411].
- [20] S. Catani and M. H. Seymour, JHEP **9907**, 023 (1999) [hep-ph/9905424].
- [21] M. Beneke, Y. Kiyo and K. Schuller, arXiv:1312.4791 [hep-ph].
- [22] P. Marquard, J. H. Piclum, D. Seidel and M. Steinhauser, Phys. Rev. D **89**, 034027 (2014) [arXiv:1401.3004 [hep-ph]].
- [23] M. Beneke, Y. Kiyo, P. Marquard, A. Penin, J. Piclum, D. Seidel and M. Steinhauser, Phys. Rev. Lett. **112**, 151801 (2014) [arXiv:1401.3005 [hep-ph]].
- [24] G. Rodrigo, A. Santamaria and M. S. Bilenky, Phys. Rev. Lett. **79**, 193 (1997) [hep-ph/9703358].
- [25] P. Nason and C. Oleari, Phys. Lett. B **407**, 57 (1997) [hep-ph/9705295].
- [26] A. Brandenburg and P. Uwer, Nucl. Phys. B **515**, 279 (1998) [hep-ph/9708350].
- [27] P. Nason and C. Oleari, Nucl. Phys. B **521**, 237 (1998) [hep-ph/9709360].
- [28] G. Rodrigo, M. S. Bilenky and A. Santamaria, Nucl. Phys. B **554**, 257 (1999) [hep-ph/9905276].
- [29] W. Bernreuther, R. Bonciani, T. Gehrmann, R. Heinesch, T. Leineweber, P. Mastrolia and E. Remiddi, Nucl. Phys. B **706**, 245 (2005) [hep-ph/0406046].

- [30] W. Bernreuther, R. Bonciani, T. Gehrmann, R. Heinesch, T. Leineweber, P. Mastrolia and E. Remiddi, Nucl. Phys. B **712**, 229 (2005) [hep-ph/0412259].
- [31] W. Bernreuther, R. Bonciani, T. Gehrmann, R. Heinesch, T. Leineweber and E. Remiddi, Nucl. Phys. B **723**, 91 (2005) [hep-ph/0504190].
- [32] J. Gluza, A. Mitov, S. Moch and T. Riemann, JHEP **0907**, 001 (2009) [arXiv:0905.1137 [hep-ph]].
- [33] K. Fabricius, I. Schmitt, G. Kramer and G. Schierholz, Z. Phys. C **11** (1981) 315.
- [34] G. Kramer and B. Lampe, Fortsch. Phys. **37**, 161 (1989).
- [35] H. Baer, J. Ohnemus and J. F. Owens, Phys. Rev. D **40**, 2844 (1989).
- [36] W. T. Giele and E. W. N. Glover, Phys. Rev. D **46**, 1980 (1992).
- [37] W. T. Giele, E. W. N. Glover and D. A. Kosower, Nucl. Phys. B **403**, 633 (1993) [hep-ph/9302225].
- [38] B. W. Harris and J. F. Owens, Phys. Rev. D **65**, 094032 (2002) [hep-ph/0102128].
- [39] S. Keller and E. Laenen, Phys. Rev. D **59**, 114004 (1999) [hep-ph/9812415].
- [40] R. K. Ellis, D. A. Ross and A. E. Terrano, Nucl. Phys. B **178**, 421 (1981).
- [41] M. L. Mangano, P. Nason and G. Ridolfi, Nucl. Phys. B **373**, 295 (1992).
- [42] Z. Kunszt and D. E. Soper, Phys. Rev. D **46**, 192 (1992).
- [43] S. Frixione, Z. Kunszt and A. Signer, Nucl. Phys. B **467**, 399 (1996) [hep-ph/9512328].
- [44] S. Catani and M. H. Seymour, Nucl. Phys. B **485**, 291 (1997) [Erratum-ibid. B **510**, 503 (1998)] [hep-ph/9605323].
- [45] S. Catani, S. Dittmaier, M. H. Seymour and Z. Trocsanyi, Nucl. Phys. B **627**, 189 (2002) [hep-ph/0201036].
- [46] A. Gehrmann-De Ridder, T. Gehrmann, E. W. N. Glover and J. Pires, Phys. Rev. Lett. **110**, no. 16, 162003 (2013) [arXiv:1301.7310 [hep-ph]].
- [47] J. Currie, A. Gehrmann-De Ridder, E. W. N. Glover and J. Pires, JHEP **1401**, 110 (2014) [arXiv:1310.3993 [hep-ph]].
- [48] Z. Bern, L. J. Dixon and D. A. Kosower, JHEP **0001**, 027 (2000) [hep-ph/0001001].
- [49] V. A. Smirnov, Phys. Lett. B **460**, 397 (1999) [hep-ph/9905323].
- [50] J. B. Tausk, Phys. Lett. B **469**, 225 (1999) [hep-ph/9909506].
- [51] C. Anastasiou, T. Gehrmann, C. Oleari, E. Remiddi and J. B. Tausk, Nucl. Phys. B **580**, 577 (2000) [hep-ph/0003261].

- [52] C. Anastasiou, E. W. N. Glover, C. Oleari and M. E. Tejeda-Yeomans, Nucl. Phys. B **601**, 318 (2001) [hep-ph/0010212].
- [53] C. Anastasiou, E. W. N. Glover, C. Oleari and M. E. Tejeda-Yeomans, Nucl. Phys. B **601**, 341 (2001) [hep-ph/0011094].
- [54] C. Anastasiou, E. W. N. Glover, C. Oleari and M. E. Tejeda-Yeomans, Phys. Lett. B **506**, 59 (2001) [hep-ph/0012007].
- [55] C. Anastasiou, E. W. N. Glover, C. Oleari and M. E. Tejeda-Yeomans, Nucl. Phys. B **605**, 486 (2001) [hep-ph/0101304].
- [56] E. W. N. Glover, C. Oleari and M. E. Tejeda-Yeomans, Nucl. Phys. B **605**, 467 (2001) [hep-ph/0102201].
- [57] E. W. N. Glover and M. E. Tejeda-Yeomans, JHEP **0105**, 010 (2001) [hep-ph/0104178].
- [58] T. Binoth and G. Heinrich, Nucl. Phys. B **585**, 741 (2000) [hep-ph/0004013].
- [59] S. Weinzierl, JHEP **0303**, 062 (2003) [hep-ph/0302180].
- [60] S. Weinzierl, JHEP **0307**, 052 (2003) [hep-ph/0306248].
- [61] C. Anastasiou, K. Melnikov and F. Petriello, Phys. Rev. D **69**, 076010 (2004) [hep-ph/0311311].
- [62] T. Binoth and G. Heinrich, Nucl. Phys. B **693**, 134 (2004) [hep-ph/0402265].
- [63] C. Anastasiou, K. Melnikov and F. Petriello, Phys. Rev. Lett. **93**, 032002 (2004) [hep-ph/0402280].
- [64] A. Gehrmann-De Ridder, T. Gehrmann and E. W. N. Glover, Nucl. Phys. B **691**, 195 (2004) [hep-ph/0403057].
- [65] C. Anastasiou, K. Melnikov and F. Petriello, Phys. Rev. Lett. **93**, 262002 (2004) [hep-ph/0409088].
- [66] S. Frixione and M. Grazzini, JHEP **0506**, 010 (2005) [hep-ph/0411399].
- [67] G. Somogyi, Z. Trocsanyi and V. Del Duca, JHEP **0506**, 024 (2005) [hep-ph/0502226].
- [68] A. Gehrmann-De Ridder, T. Gehrmann and E. W. N. Glover, JHEP **0509**, 056 (2005) [hep-ph/0505111].
- [69] K. Melnikov and F. Petriello, Phys. Rev. Lett. **96**, 231803 (2006) [hep-ph/0603182].
- [70] G. Somogyi, Z. Trocsanyi and V. Del Duca, JHEP **0701**, 070 (2007) [hep-ph/0609042].
- [71] G. Somogyi and Z. Trocsanyi, JHEP **0701**, 052 (2007) [hep-ph/0609043].
- [72] S. Catani and M. Grazzini, Phys. Rev. Lett. **98**, 222002 (2007) [hep-ph/0703012].

- [73] A. Gehrmann-De Ridder, T. Gehrmann, E. W. N. Glover and G. Heinrich, JHEP **0711**, 058 (2007) [arXiv:0710.0346 [hep-ph]].
- [74] A. Gehrmann-De Ridder, T. Gehrmann, E. W. N. Glover and G. Heinrich, Phys. Rev. Lett. **100**, 172001 (2008) [arXiv:0802.0813 [hep-ph]].
- [75] G. Somogyi and Z. Trocsanyi, JHEP **0808**, 042 (2008) [arXiv:0807.0509 [hep-ph]].
- [76] S. Weinzierl, Phys. Rev. Lett. **101**, 162001 (2008) [arXiv:0807.3241 [hep-ph]].
- [77] K. Melnikov, Phys. Lett. B **666**, 336 (2008) [arXiv:0803.0951 [hep-ph]].
- [78] U. Aglietti, V. Del Duca, C. Duhr, G. Somogyi and Z. Trocsanyi, JHEP **0809**, 107 (2008) [arXiv:0807.0514 [hep-ph]].
- [79] S. Catani, L. Cieri, G. Ferrera, D. de Florian and M. Grazzini, Phys. Rev. Lett. **103**, 082001 (2009) [arXiv:0903.2120 [hep-ph]].
- [80] S. Weinzierl, JHEP **0907**, 009 (2009) [arXiv:0904.1145 [hep-ph]].
- [81] P. Bolzoni, S. O. Moch, G. Somogyi and Z. Trocsanyi, JHEP **0908**, 079 (2009) [arXiv:0905.4390 [hep-ph]].
- [82] A. Daleo, A. Gehrmann-De Ridder, T. Gehrmann and G. Luisoni, JHEP **1001**, 118 (2010) [arXiv:0912.0374 [hep-ph]].
- [83] E. W. Nigle Glover and J. Pires, JHEP **1006**, 096 (2010) [arXiv:1003.2824 [hep-ph]].
- [84] S. Biswas and K. Melnikov, JHEP **1002**, 089 (2010) [arXiv:0911.4142 [hep-ph]].
- [85] P. Bolzoni, F. Maltoni, S. O. Moch and M. Zaro, Phys. Rev. Lett. **105**, 011801 (2010) [arXiv:1003.4451 [hep-ph]].
- [86] M. Czakon, Phys. Lett. B **693**, 259 (2010) [arXiv:1005.0274 [hep-ph]].
- [87] P. Bolzoni, G. Somogyi and Z. Trocsanyi, JHEP **1101**, 059 (2011) [arXiv:1011.1909 [hep-ph]].
- [88] R. Boughezal, A. Gehrmann-De Ridder and M. Ritzmann, JHEP **1102**, 098 (2011) [arXiv:1011.6631 [hep-ph]].
- [89] M. Czakon, Nucl. Phys. B **849**, 250 (2011) [arXiv:1101.0642 [hep-ph]].
- [90] W. Bernreuther, C. Bogner and O. Dekkers, JHEP **1106**, 032 (2011) [arXiv:1105.0530 [hep-ph]].
- [91] T. Gehrmann and P. F. Monni, JHEP **1112**, 049 (2011) [arXiv:1107.4037 [hep-ph]].
- [92] G. Ferrera, M. Grazzini and F. Tramontano, Phys. Rev. Lett. **107**, 152003 (2011) [arXiv:1107.1164 [hep-ph]].
- [93] C. Anastasiou, F. Herzog and A. Lazopoulos, JHEP **1203**, 035 (2012) [arXiv:1110.2368 [hep-ph]].

- ph]].
- [94] S. Catani, L. Cieri, D. de Florian, G. Ferrera and M. Grazzini, Phys. Rev. Lett. **108**, 072001 (2012) [arXiv:1110.2375 [hep-ph]].
 - [95] G. Abelof and A. Gehrmann-De Ridder, JHEP **1204**, 076 (2012) [arXiv:1112.4736 [hep-ph]].
 - [96] P. Brnreuther, M. Czakon and A. Mitov, Phys. Rev. Lett. **109**, 132001 (2012) [arXiv:1204.5201 [hep-ph]].
 - [97] A. Gehrmann-De Ridder, T. Gehrmann and M. Ritzmann, JHEP **1210**, 047 (2012) [arXiv:1207.5779 [hep-ph]].
 - [98] G. Abelof and A. Gehrmann-De Ridder, JHEP **1211**, 074 (2012) [arXiv:1207.6546 [hep-ph]].
 - [99] J. Gao, C. S. Li and H. X. Zhu, Phys. Rev. Lett. **110**, 042001 (2013) [arXiv:1210.2808 [hep-ph]].
 - [100] G. Abelof, O. Dekkers and A. Gehrmann-De Ridder, JHEP **1212**, 107 (2012) [arXiv:1210.5059 [hep-ph]].
 - [101] J. Currie, E. W. N. Glover and S. Wells, JHEP **1304**, 066 (2013) [arXiv:1301.4693 [hep-ph]].
 - [102] M. Brucherseifer, F. Caola and K. Melnikov, JHEP **1304**, 059 (2013) [arXiv:1301.7133 [hep-ph]].
 - [103] R. Boughezal, F. Caola, K. Melnikov, F. Petriello and M. Schulze, JHEP **1306**, 072 (2013) [arXiv:1302.6216 [hep-ph]].
 - [104] M. Czakon, P. Fiedler and A. Mitov, Phys. Rev. Lett. **110**, no. 25, 252004 (2013) [arXiv:1303.6254 [hep-ph]].
 - [105] W. Bernreuther, C. Bogner and O. Dekkers, JHEP **1310**, 161 (2013) [arXiv:1309.6887 [hep-ph]].
 - [106] M. Grazzini, S. Kallweit, D. Rathlev and A. Torre, Phys. Lett. B **731**, 204 (2014) [arXiv:1309.7000 [hep-ph]].
 - [107] L. Liu-Sheng, Z. Ren-You, M. Wen-Gan, G. Lei, L. Wei-Hua and L. Xiao-Zhou, Phys. Rev. D **89**, 073001 (2014) [arXiv:1401.7754 [hep-ph]].
 - [108] G. Abelof, A. Gehrmann-De Ridder, P. Maierhofer and S. Pozzorini, arXiv:1404.6493 [hep-ph].
 - [109] M. Brucherseifer, F. Caola and K. Melnikov, arXiv:1404.7116 [hep-ph].
 - [110] F. Cascioli, T. Gehrmann, M. Grazzini, S. Kallweit, P. Maierhofer, A. von Manteuffel, S. Pozzorini and D. Rathlev *et al.*, arXiv:1405.2219 [hep-ph].

- [111] C. Anastasiou, J. Cancino, F. Chavez, C. Duhr, A. Lazopoulos, B. Mistlberger and R. Mueller, arXiv:1408.4546 [hep-ph].
- [112] A. H. Hoang, M. Jezabek, J. H. Kuhn and T. Teubner, Phys. Lett. B **338**, 330 (1994) [hep-ph/9407338].
- [113] K. G. Chetyrkin, A. H. Hoang, J. H. Kuhn, M. Steinhauser and T. Teubner, In *An-necy/Assergi/Hamburg 1995, e+ e- collisions at TeV energies, pt. B* 29-32 [hep-ph/9605311].
- [114] A. H. Hoang, J. H. Kuhn and T. Teubner, Nucl. Phys. B **452**, 173 (1995) [hep-ph/9505262].
- [115] A. H. Hoang and T. Teubner, Nucl. Phys. B **519**, 285 (1998) [hep-ph/9707496].
- [116] C. W. Bauer, D. Pirjol and I. W. Stewart, Phys. Rev. D **65**, 054022 (2002) [hep-ph/0109045].
- [117] T. Becher, M. Neubert and B. D. Pecjak, JHEP **0701**, 076 (2007) [hep-ph/0607228].
- [118] S. A. Larin, T. van Ritbergen and J. A. M. Vermaseren, Nucl. Phys. B **438**, 278 (1995) [hep-ph/9411260].
- [119] K. G. Chetyrkin, B. A. Kniehl and M. Steinhauser, Phys. Rev. Lett. **79**, 2184 (1997) [hep-ph/9706430].
- [120] K. G. Chetyrkin, B. A. Kniehl and M. Steinhauser, Nucl. Phys. B **510**, 61 (1998) [hep-ph/9708255].
- [121] K. G. Chetyrkin, J. H. Kuhn and M. Steinhauser, Comput. Phys. Commun. **133**, 43 (2000) [hep-ph/0004189].
- [122] A. Mitov and S. Moch, JHEP **0705**, 001 (2007) [hep-ph/0612149].
- [123] E. Remiddi and J. A. M. Vermaseren, Int. J. Mod. Phys. A **15**, 725 (2000) [hep-ph/9905237].
- [124] T. Gehrmann and E. Remiddi, Comput. Phys. Commun. **141**, 296 (2001) [hep-ph/0107173].
- [125] A. von Manteuffel, R. M. Schabinger, H. X. Zhu, “The two-loop soft function for heavy quark pair production at future linear colliders”, in press.
- [126] G. P. Korchemsky and A. V. Radyushkin, Nucl. Phys. B **283**, 342 (1987).
- [127] N. Kidonakis, Phys. Rev. Lett. **102**, 232003 (2009) [arXiv:0903.2561 [hep-ph]].
- [128] T. Becher and M. Neubert, Phys. Rev. D **79**, 125004 (2009) [Erratum-ibid. D **80**, 109901 (2009)] [arXiv:0904.1021 [hep-ph]].
- [129] S. Catani, S. Dittmaier, M. H. Seymour and Z. Trocsanyi, Nucl. Phys. B **627**, 189 (2002) [hep-ph/0201036].
- [130] G. Cullen, H. van Deurzen, N. Greiner, G. Heinrich, G. Luisoni, P. Mastrolia, E. Mirabella and G. Ossola *et al.*, arXiv:1404.7096 [hep-ph].

- [131] P. Mastrolia, E. Mirabella and T. Peraro, JHEP **1206**, 095 (2012) [Erratum-ibid. **1211**, 128 (2012)] [arXiv:1203.0291 [hep-ph]].
- [132] T. Peraro, Comput. Phys. Commun. **185**, 2771 (2014) [arXiv:1403.1229 [hep-ph]].
- [133] A. van Hameren, C. G. Papadopoulos and R. Pittau, JHEP **0909**, 106 (2009) [arXiv:0903.4665 [hep-ph]].
- [134] A. van Hameren, Comput. Phys. Commun. **182**, 2427 (2011) [arXiv:1007.4716 [hep-ph]].
- [135] E. Laenen, L. Magnea, G. Stavenga and C. D. White, Nucl. Phys. Proc. Suppl. **205-206**, 260 (2010) [arXiv:1007.0624 [hep-ph]].
- [136] E. Laenen, L. Magnea, G. Stavenga and C. D. White, JHEP **1101**, 141 (2011) [arXiv:1010.1860 [hep-ph]].
- [137] K. G. Chetyrkin, J. H. Kuhn and M. Steinhauser, Nucl. Phys. B **482**, 213 (1996) [hep-ph/9606230].
- [138] A. Denner and T. Sack, Nucl. Phys. B **358**, 46 (1991).
- [139] J. Beringer *et al.* [Particle Data Group Collaboration], Phys. Rev. D **86**, 010001 (2012).
- [140] S. Höche, Y. Li and S. Prestel, arXiv:1405.3607 [hep-ph].
- [141] S. Höche, Y. Li and S. Prestel, arXiv:1407.3773 [hep-ph].

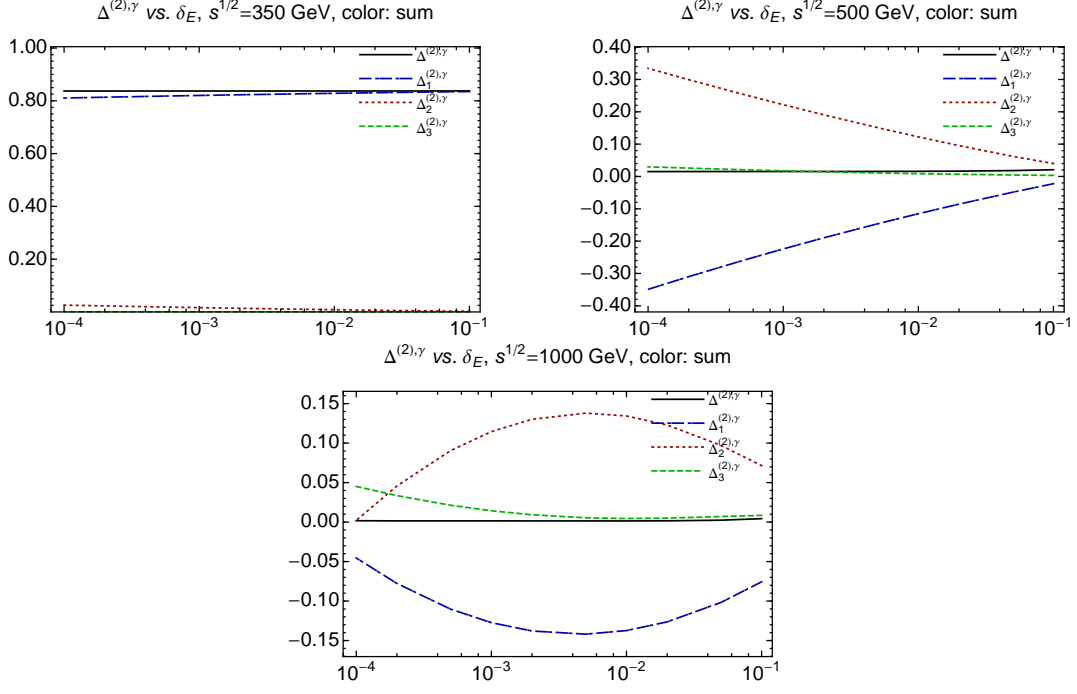


FIG. 1: Dependence of separate contributions to $\Delta^{(2),\gamma}$ with full colors on the cut-off for different collision energies.

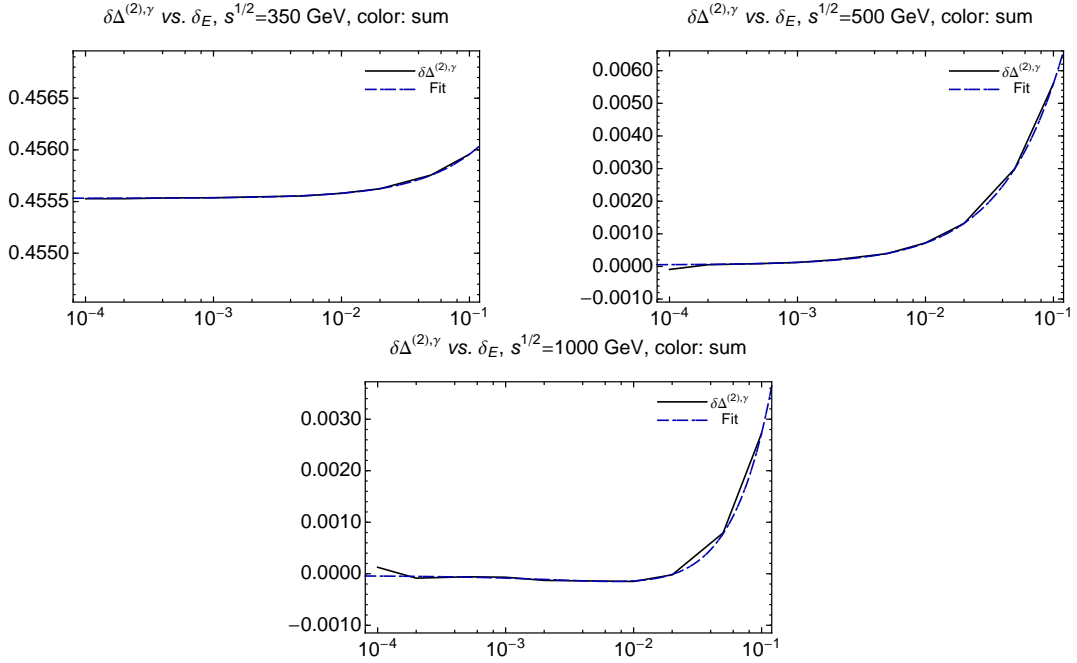


FIG. 2: Dependence of $\delta\Delta^{(2),\gamma}$ with full colors on the cut-off and the fitted curves for different collision energies.

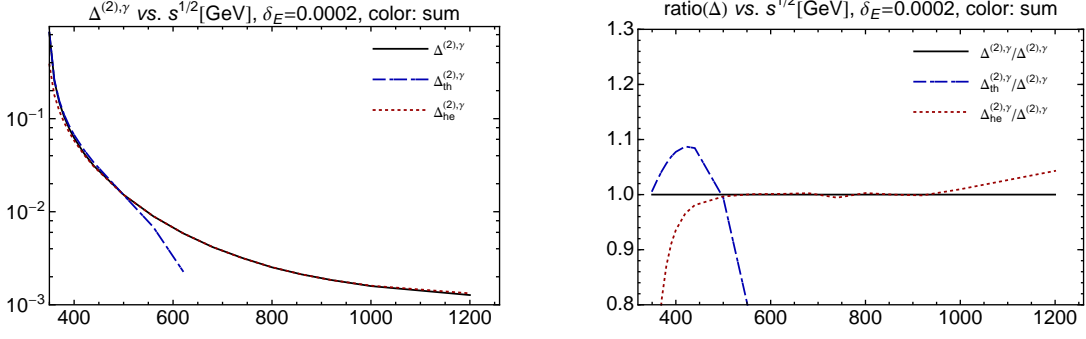


FIG. 3: Comparison of $\Delta^{(2),\gamma}$ with the threshold results $\Delta_{th}^{(2),\gamma}$ and high-energy expansion results $\Delta_{he}^{(2),\gamma}$ in terms of their absolute values and ratios.

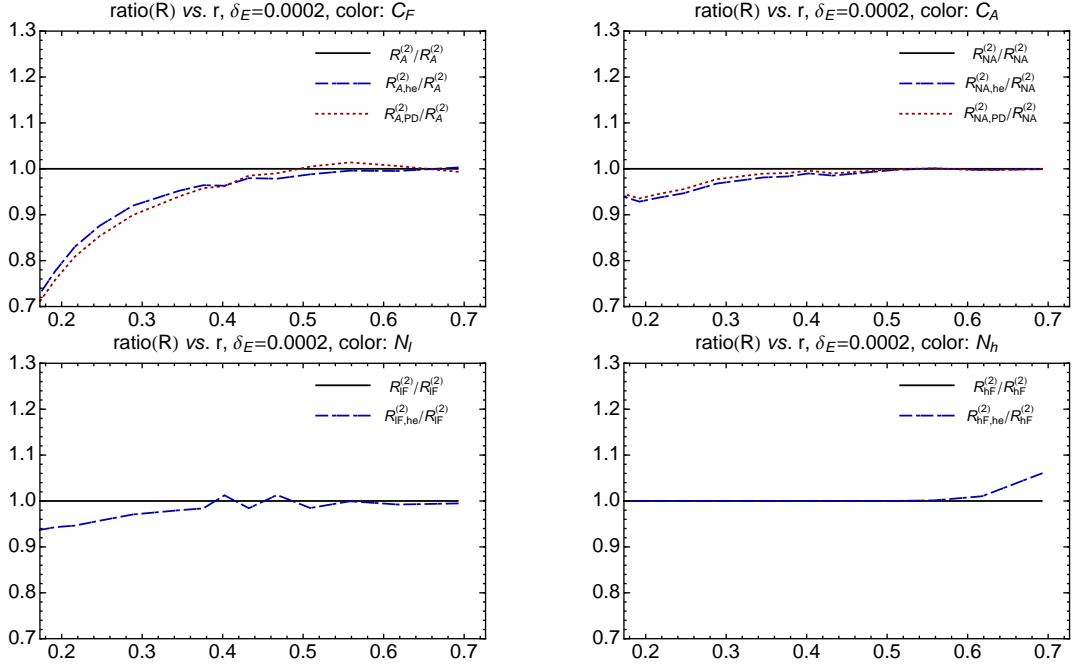


FIG. 4: Comparison of different color structures of $R^{(2)}$ with the high-energy expansion $R_{he}^{(2)}$ and Padé approximation $R_{PD}^{(2)}$ in the high-energy region.

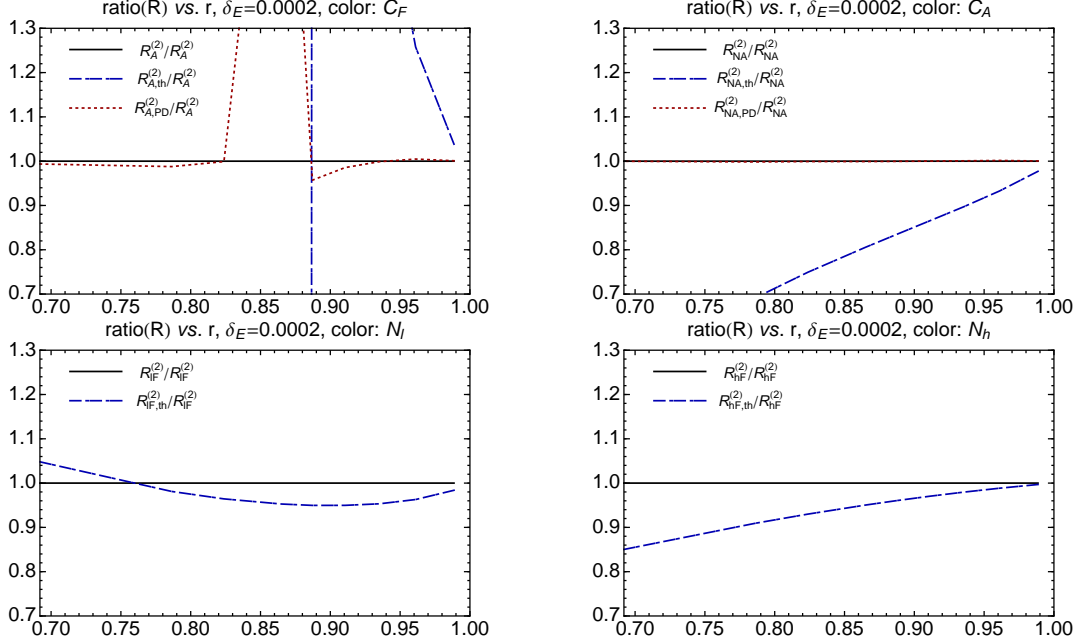


FIG. 5: Comparison of different color structures of $R^{(2)}$ with the threshold results $R_{th}^{(2)}$ and Padé approximation $R_{PD}^{(2)}$ in the threshold region.

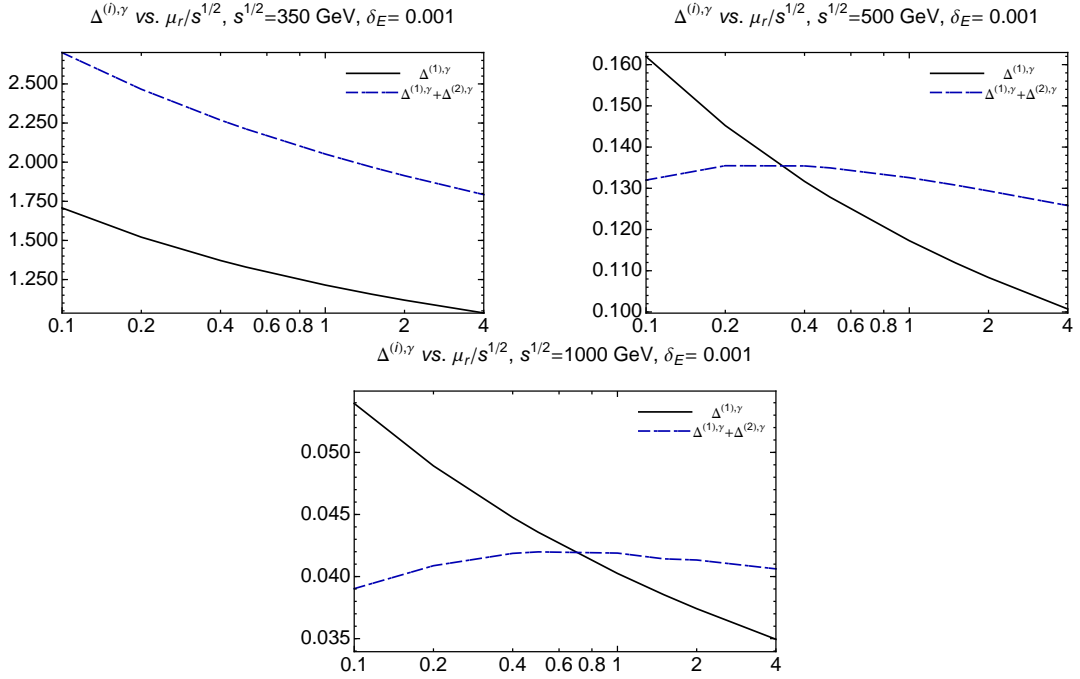


FIG. 6: Scale dependence of $\Delta^{(1),\gamma}$ and $\Delta^{(1),\gamma} + \Delta^{(2),\gamma}$ for different collision energies.

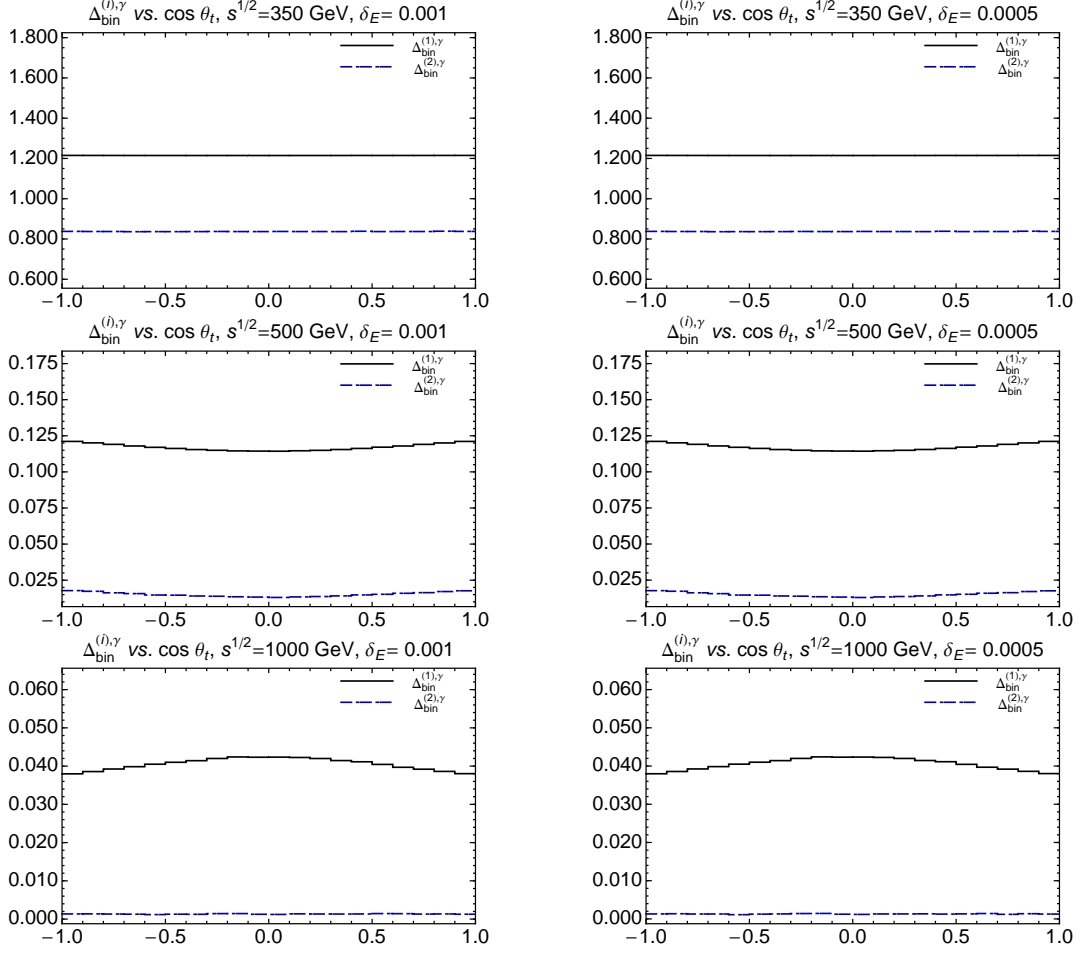


FIG. 7: $\mathcal{O}(\alpha_s)$ and $\mathcal{O}(\alpha_s^2)$ corrections in different $\cos \theta_t$ bins, $\Delta_{bin}^{(1),\gamma}$ and $\Delta_{bin}^{(2),\gamma}$ for different collision energies and different δ_E choices.

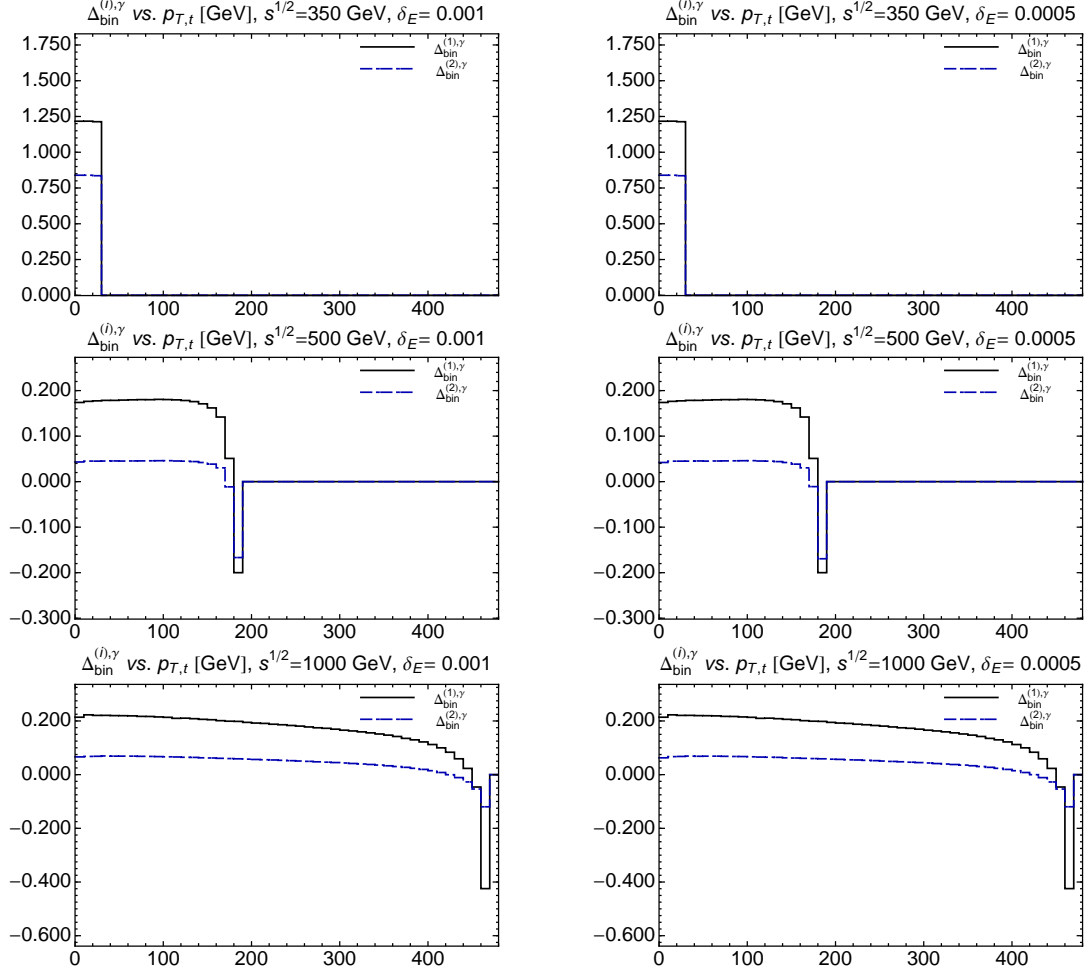


FIG. 8: NLO and NNLO corrections in different $p_{T,t}$ bins, $\Delta_{bin}^{(1),\gamma}$ and $\Delta_{bin}^{(2),\gamma}$, for different collision energies and different δ_E choices.

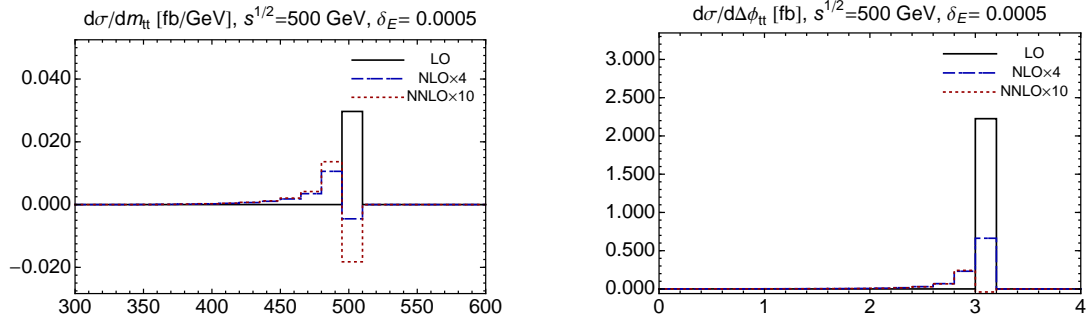


FIG. 9: Differential distribution, $d\sigma/dm_{t\bar{t}}$ on left, $d\sigma/d\Delta\phi_{t\bar{t}}$ on right, at the LO, $\mathcal{O}(\alpha_s)$ (multiplied by 4), and $\mathcal{O}(\alpha_s^2)$ (multiplied by 10).